Next Materials 7 (2025) 100373

Contents lists available at ScienceDirect

Next Materials

journal homepage: www.sciencedirect.com/journal/next-materials

Research article

Engineered silica NPs to hold and release the antimicrobial product Biotin T ®

Andrea Campostrini [a], Elena Ghedini [a,*], Teresa Botrè [a], Sabrina Manente [a], Alessia Giordana [b], Giuseppina Cerrato [b], Giuseppe Cruciani [c], Alex W. Robertson [d], Michela Signoretto [a], Federica Menegazzo [a]

[a] Department of Molecular Sciences and Nanosystems, Ca' Foscari University of Venice, Via Torino 155, Venice 30172, Italy
[b] Chemistry Department, University of Turin and NIS Interdept. Centre, Via P. Giuria 7, Turin 10125, Italy
[c] Physics and Earth Sciences Department, University of Ferrara, Via Giuseppe Saragat, 1, Ferrara 44122, Italy
[d] Department of Physics, University of Warwick, Coventry CV4 7AL, United Kingdom

ARTICLE INFO

Keywords:
Silica nanoparticles
Sulphonic group
Biotin T
Antimicrobial
Cultural heritage

ABSTRACT

While the preservation of culturally significant materials is increasingly recognized as important within the scientific community, it remains closely tied to traditional practices and the empiric knowledge of small handicraft companies. These procedures are usually highly effective, but, especially when dealing with biological degradation phenomena, they are often not updated to the latest scientific innovations and hence do not always consider the impact of their use on the environment. MCM-41 silica-based nanoparticles were employed as nanocontainers to encapsulate and later release the antimicrobial agent Biotin T ®. Specifically, the silica nanoparticles were modified with sulphonic groups to functionalize the silica structure and its interaction with the antimicrobial compound, thereby aiming to regulate its release. Microbiological tests were conducted to determine Biotin T ® antimicrobial activity at low concentrations. The nanomaterials were characterized by N_2 physisorption, XRD, TPO, TG/TDA, Raman IR/ATR spectroscopy, SEM, EDS, and HR-TEM, whereas Biotin T ® release was studied through UV spectroscopy. The functionalized silica nanoparticle-based matrix can encapsulate and gradually release the commercial biocidal. Two of the matrices, MCM-41 and MCM-SO_3H, exhibited different properties after functionalization, with both maintaining the original structure but leading to a higher interaction with the antimicrobial product.

1. Introduction

Stone cultural heritage materials are often subject to degradation phenomena that are related to the environment they are exposed to. It is hence crucial to protect them and to improve the products employed to reduce the degradation effects [1–3].

Biodegradation is considered one of the most dangerous factors that could alter the material conservation state; it has a high aesthetical negative impact and can be one of the first steps of a series of more complex phenomena that could lead to the complete loss of the artwork [4–6].

Various methods to remove environmental deposits and restore the original surface are currently employed; however, they primarily imply the application of products only once the material has already been highly colonized and/or damaged [7,8]. Antimicrobial commercial products are hence usually applied for cleaning interventions, without considering their potential preventive power [9]. Numerous products are employed in the cleaning and preventing interventions in the field of conservation and restoration; one of the most commonly used for the treatment of stone surfaces has the commercial name of "Biotin T", which is normally employed for cleaning interventions at low concentrations, around 1–3 % [10,11]. Its composition is based on two components: a quaternary ammonium salt (didecyldimethylammonium chloride – DDAC) and the molecule of 2-octyl-2 H-isothiazol-3-one (OIT), reported in Fig. 1; their action is respectively related to fungicide and antimicrobic actions [12–14].

Subsequent to a cleaning intervention, a protective coating should be applied to minimize further attacks on the stone surface, provided that it must not alter the surface properties or chromatic characteristics of the substrate [15–17].

* Corresponding author.
E-mail address: gelena@unive.it (E. Ghedini).

https://doi.org/10.1016/j.nxmate.2024.100373
Received 27 May 2024; Received in revised form 3 September 2024; Accepted 9 September 2024
Available online 16 September 2024

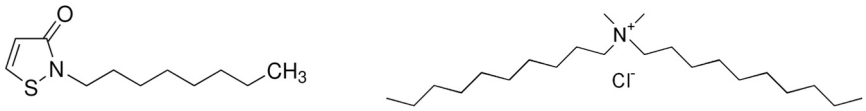

(a) 2-octyl-2H-isothiazol-3-one (OIT) (b) Didecyldimethylammonium chloride (DDAC)

Fig. 1. Biotin T ® main active molecules: 2-octyl-2 H-isothiazol-3-one (a), and Didecyldimethylammonium chloride (b).

Nanostructured protective coatings are typically employed for this aim, exploiting the appealing features of nanomaterials [18–22]. Nanoparticles (NPs), usually metal oxides, have been studied since the 80 s for their applications in conservation science. This growing interest is related to the high chemical and aesthetical compatibility that these materials have. Moreover, they can present lower toxicity towards the environment and the operator [23]. The presence of NPs on the surface could have both a chemical and a physical effect; the NPs' elevated surface area ratio can confer the material with high reactivity, which could lead to favorable interaction with the environment, such as self-cleaning features. From a physical point of view, instead, the NPs' presence could enhance the surface hydrophobicity, creating a micro-roughness that could lead water to form droplets over the surface instead of being absorbed by the material. Other appealing characteristics are related to the possibility of modifying their properties by changing the porosity, size, and shape or grafting them with functional groups. Nanoparticles that are highly functionalizable and present the just reported characteristics are hence widely employed in several fields, such as in the development of hi-tech conveying systems of biologically active molecules.

Embedding active substances in nanosized materials to control their release is a well-known technique, in what is generally referred to as Drug Delivery System (DDS). Indeed, the term DDS is usually used to describe the conveying of bioactive molecules, such as drugs, in a controlled and targeted way. It is an application that is highly employed in the medical and pharmaceutical fields, but which can be employed in many other sectors. These kinds of systems can grant to the formulation a modulated release over time, regulating its kinetic to maximize the efficiency and reducing the number of treatments, and hence the costs [24–26].

Matrices are fundamental in the formulation of a DDS because they are responsible for controlling the release of the active molecule, which might be modulated both by chemical and/or physical interactions. Matrices' parameters can also be modified to further vary the release control by changing the structure and the material morphology, surface functional groups, material degradation, material hydrophobicity or hydrophilicity, or even the capability to interact with the active substance without modifying its activity.

In this field, particularly noteworthy are porous silica nanoparticles (SiO_2 NPs), which have been widely employed to encapsulate biomolecules and enzymes in different fields of application [27,28]; these matrices exhibit high biocompatibility and biodegradability, resistance to microbial attacks, and are characterized by high mechanical strength, elevated thermal stability, and negligible swelling in organic solvents compared to organic polymers. These features contribute to making this type of material an excellent carrier in many systems, including biological ones, as they allow reaching the target without degradation and protect the active agent until it is released to perform its function [29–31]. For these materials, a high surface area, a large pore volume, and an appropriate size of the pores are essential requirements to encapsulate a desired amount of the active substance. Through the appropriate modification of these parameters, it is possible to modulate the loading and release of the active ingredient [32–35].

Mesoporous silicas, such as MCM-41 and SBA-15, are highly efficient matrices in the design of a controlled release system, owing to features such as pore size and their ordered structure [36–40].

The surface area of mesoporous silicas is composed of the sum of the external and porous surface areas. Its high value (approximately 700–1000 m^2/g) results in a significant reactivity of the material, allowing for the encapsulation of a large quantity of molecules within it [41]. Silica contains silanol groups (Si-OH), and increasing the temperature leads to their disappearance [42]. Therefore, subjecting silica to high temperatures enhances its hydrophobic character. In this scenario, the adsorption process is characterized by hydrophobic van der Waals dispersive forces. Another intriguing aspect concerning the surface of silicas is that upon contact with aqueous solutions of varying ionic strength and pH, silanols can undergo deprotonation, resulting in a negative surface charge (SiO^-) that facilitates the adsorption of ions and polar molecules from the solution [43].

The ability to modify the surface of silica is a key feature that makes this material highly versatile. It is possible to tailor material characteristics according to specific needs by introducing a wide variety of functional groups. These functional groups may include amines, thiols, carboxyl, or sulfonic groups. Functionalization is a common procedure when aiming to modulate the properties of controlled release in mesoporous silicas for DDS. The goal is to enhance the interaction between the functional groups of the matrix and the active agent incorporated within it. The two most commonly employed procedures for functionalization are co-condensation and grafting. These techniques, depending on the application field, enable the modification of the matrix to enhance its interaction with the molecule to be transported.

Hence, the incorporation of the biocide within the pores of the grafted silica matrix would allow for its controlled release over time, thereby reducing the frequency of cleaning interventions on the surface of the target stone. Furthermore, by maximizing the interaction with the biocide and modulating its release, the proliferation of microorganisms' colonies over the stone surface would be avoided or at least reduced. Additionally, the use of silica nanocapsules in a protective coating would also contribute to modulating its final properties, enhancing, for example, its hydrophobicity.

Therefore, the goal of this study is to functionalize silica nanoparticles with sulphonic functional groups, aiming to modulate the release by modifying the silica matrix structure and its interaction with the antimicrobic commercial product Biotin T ®. In particular, attention was focused on MCM-41 silica NPs.

2. Materials and methods

2.1. MCM-41 synthesis

Mesoporous MCM-41 was synthesized using TEOS (Tetraethyl orthosilicate; CAS 78–10–4) as the silica source and hexadecyltrimethylammonium bromide (CTAB; CAS 57–09–0) as the template in NaOH (CAS 1310–73–2) basic solution. The mixture was continuously stirred at 300 rpm for 3 h at 25 °C and crystallized in a Teflon autoclave at 75 °C for 70 h, keeping pH = 11. The mixture was then filtered, washed, dried at 25 °C for 20 h, and finally calcined in air (50 mL/min) at 510 °C (0.5 °C/min rate) for 6 hours.

All the materials employed for this step were purchased from Sigma-Aldrich® (Merck Life Science S.r.l., Milan, Italy).

2.2. MCM-41 grafting with -SO_3H groups

A post-grafting method was used to functionalize the above MCM-41 material, following the procedure reported by previous work from the authors [44]. (3-Mercaptopropyl)trimethoxysilane (MPTMS; CAS

4420–74–0) was used as grafting agent and a NaCl (CAS 7647–14–5) solution 0.2 M was used as reaction solvent: 1 g of MCM-41 was dissolved in 30 mL of saline solution. MPTMS was added to the mixture exhibiting a 2:1 M ratio of SiO_2 to 1 MPTMS and the mixture was stirred at 1000 rpm for 24 h at 90 °C. The solid was then washed in water (three portions of 20 mL) and dried for 18 h at 70 °C. The material was labeled MCM-SH. Then, mild oxidation with 30 wt% H_2O_2 (CAS 7722–84–1) using a 2:0.11 M ratio of SiO_2 to H_2O_2 was performed stirring at 500 rpm for 24 h at 30 °C. The sulfonated solid was filtered, washed with methanol (CAS 67–56–1), and dried at RT for 18 h. The final material was labeled MCM-SO_3H.

All the materials employed for this step were purchased from Sigma-Aldrich® (Merck Life Science S.r.l., Milan, Italy).

2.3. Impregnation with Biotin T ®

The nanomaterials MCM-41 and MCM-SO_3H were impregnated by Incipient Wetness Impregnation (IWI) method with an aqueous solution of Biotin T ® 30 %. In order to ensure optimal impregnation of the biocide, a series of intermediate drying steps at 30 °C were carried out. The silica matrices were both impregnated with Biotin T ® till the maximum of their absorption capability, leading to a concentration of Biotin T ® equal to 1.3 mL/g for MCM-41 and 0.5 mL/g for MCM-SO_3H. The two samples were respectively labeled MCM-41-BT and MCM-SO_3H-BT.

The antimicrobial product Biotin T ® was purchased from CTS S.r.l., Altavilla Vicentina, Italy.

2.4. Microbiological sampling campaign

To select the microorganisms to be used, a sampling campaign has been conducted on real-case built heritage stone materials present in the city of Venice, Italy; precisely, from the Istria stone well in *Campo dei Frari (Sestiere San Polo)* and from the external wall of *San Giacomo dall'Orio* Church *(Sestiere Santa Croce)* – IX century.

The samplings were carried out by non-invasive methods performed with adhesive tape *Fungi-Tape*™ (Fisher Scientific) and sterile cotton swabs. The samplings were directly plated on Petri dishes with Malt Extract Agar (MEA, Biolife). The Petri dishes were incubated at 21.5 ± 2 °C for 7 days for initial mycelium development and then monitored for fungal colony utilization until maturation (active and abundant sporulation) of the fungal colonies. At this stage, it was identified the Fungus *Cladosporium* sp. which was selected for this study. It was hence isolated and let grow in pure axenic culture with MEA cultivation medium for 5 days in incubator at 21.5 ± 2 °C, reaching an optimal inoculation growth level with active sporulating conidiophores.

2.5. Biotin T ® microbiological test

To test the antimicrobial properties of Biotin T ® and identify its Minimal Inhibitory Concentration (MIC), a preliminary challenge test based on the principles of the Kirby-Bauer diffusion test method was conducted [45]. The test's main intent was to assess that even a small amount of Biotin T ®, as the quantity released by the silica NPs, was sufficient to inhibit fungal growth. It is, in fact, known from literature that the encapsulation in nanomaterials does not limit the antimicrobial features of the active molecules [46].

To conduct the test, first some *Cladosporium* sp. inocula were placed in a 25 mL PBS buffer solution and vortexed for 3 minutes at 2000 rpm. Then, spore counting in the solution was performed using a Bürker counting chamber, repeating the procedure with three counting replicates ($n = 3$) to obtain an average of 5000 spores/mL [47]. Afterward, 500 µL of the spore-containing solution was taken and inoculated onto aerated Petri dishes (Ø = 90 mm) containing Malt Extract Agar (MEA – Sigma-Aldrich® Merck Life Science S.r.l., Milan, Italy) culture medium, spreading on the surface with an L-shaped loop (Hockey stick). Three sterile paper discs (Ø = 15 mm) made of cellulose pulp were then placed on each Petri dish, onto which 20 µL of Biotin T ® was absorbed at the volume concentrations of 0.1 %, 0.3 %, 1 %, 3 %, 10 %, 30 %. Petri dishes without the deposition of the biocide were also prepared and kept as references (*control*). All tests were performed in triplicate.

Depending on the growth of the Fungi, the MIC of the biocide can be determined, and thus, the amount of silica NPs required for an effective release of Biotin T ®.

To analyze the inhibition area, it was measured the average between the shorter and the largest radius of the circle where there was no fungal growth for each paper disc; then the inhibition area was calculated. The measurement was done on pictures taken at the end of the test (after 7 days) and processed through Adobe Illustrator CC software.

2.6. Characterization of the silica NPs

Specific surface areas and pore size distributions were evaluated by N_2 adsorption/desorption isotherms at −196 °C using a Tristar II Plus Micromeritics instrument. The samples underwent a pre-treatment at 70 °C prior to the analysis. The surface area was calculated using the B.E.T. method, whereas pore size distribution was determined by the B.J.H. method, applied to the N_2 desorption branch of the isotherm. For all the surface area data the error reported is lower than 2 %.

X-ray powder diffraction (XRD) analyses were carried out by a Bruker D8 Advance Da Vinci automatic diffractometer using a Cu sealed X-ray tube and equipped with a LynxEye XE strip detector with a Ni filter on the diffracted beam.

Total acid sites were determined by the following titration method: 50 mg of powder was dissolved in a 10 mL 0.02 M NaOH solution, stirring for 1 h. The contents were then filtered, diluted with 10 mL of H_2O, and then titrated with 10 mL of a 0.02 M HCl solution, using phenolphthalein as a pH indicator. The amount of acid used to titrate the solution allowed the determination of the number of acidic groups present in MCM-41 and MCM-SO_3H that reacted with NaOH.

Temperature Programmed Oxidation (TPO) measurements were carried out with an Anton Paar High Vacuum Adsorption Analyzer, autosorb iQ series C-MP. The samples (100 mg) were heated with a temperature rate of 10 °C/min from 20 to 1000 °C in a 5 % O_2/He flow (40 mL/min). The effluent gases were analyzed by a built-in TCD detector. All temperature programmed analyses were repeated twice to validate the results.

Thermal analyses (TG/DTA) were performed on a NETZSCH STA 409 PC/PG instrument in air flux (20 mL/min) using a temperature rate set at 5 °C/min in the 25–800 °C temperature range.

Raman spectra were recorded on pure samples using an FT-Raman Instrument (Bruker Vertex 70 spectrometer, equipped with the RAM II accessory and a Ge detector) by exciting with a 1064 nm Nd:YAG laser, recording 3000 scans with a resolution of 4 cm^{-1}.

Attenuated Total Reflectance (ATR) infrared spectroscopy was employed to identify the presence of IR-active vibrations attributable to functional groups that could confirm the occurrence of matrix grafting. The instrument used for the analyses is a Bruker Vertex 70 spectrometer equipped with a Harrick MVP2 ATR cell (64 scans, resolution 4 cm^{-1}), and a DTGS detector.

All data sets were processed with the software Origin 2021 by OriginLab, Northampton, MA, USA.

Scanning Electron Microscopy (SEM), coupled with Energy Dispersive X-ray Spectroscopy (EDS), and High-Resolution Transmission Electron Microscopy (HRTEM) analyses were employed to study the morphological modification of the silica matrices, to study the nanoparticles' dimensions, and to confirm the effective addition of the –SO_3H functional groups and the impregnation with the antimicrobial product. The instruments used for these analyses were a Zeis Gemini SEM with Oxford Instruments SDD EDS detector and a JEOL 2100 HRTEM with Gatan OneView detector. SEM images were acquired at an accelerating voltage of 5 kV with the secondary electron detector, and EDS maps

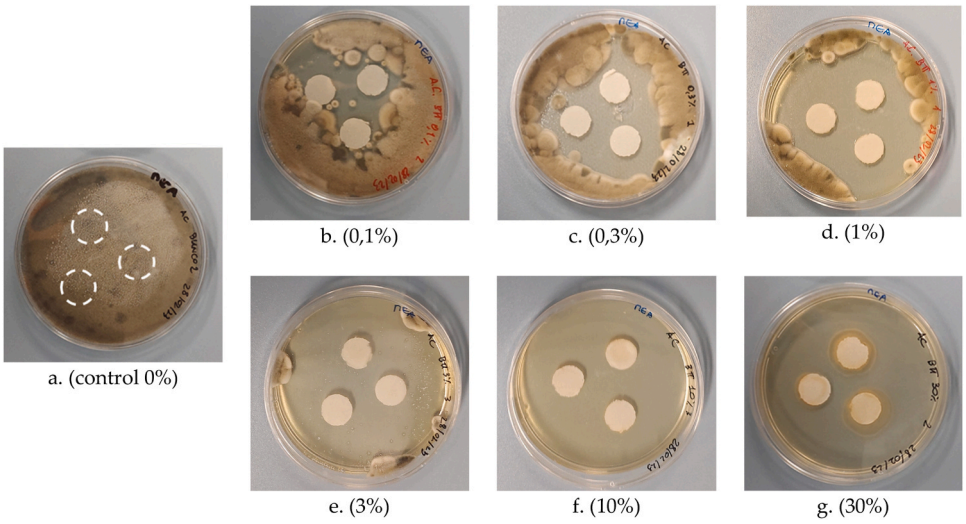

Fig. 2. Photos of the microbiological test with the different concentrations of Biotin T ®: control 0 % (a), 0.1 % (b), 0.3 % (c), 1 % (d), 3 % (e), 10 % (f), 30 % (g) – the pictures were taken after 7 days from inoculation with *Cladosporium* sp. Fungi.

were taken at an accelerating voltage of 10 kV. SEM samples were prepared by spreading a thin layer of sample powder onto sticky conducting carbon tape. HRTEM imaging was performed at an accelerating voltage of 200 kV. HRTEM samples were prepared by sonicating the sample in ethanol solvent for 5 minutes, and then subsequently drop-casting onto a holey carbon copper grid (Agar Scientific) and left to dry overnight. Data was collected using the Electron Microscopy Research Technology Platform at the University of Warwick.

2.7. Study of the release system

To evaluate the ability to release the active components of Biotin T ®, from both unmodified and grafted silica NPs, a customized release test was optimized. In this test, various aqueous solutions of MCM-41 and MCM-SO_3H of equal concentration were shaken over a time interval ranging from 30 minutes to 30 days. Subsequently, the solutions were filtered (0.2 μm filter) and analyzed using UV–visible spectrophotometry to identify and quantify the concentration of biocide molecules in the sample solutions.

The test was carried out to simulate the slower release that would take place in much more time when inserted into an antimicrobial protective coating formulation.

The powder samples of MCM-41 and MCM-SO_3 were dissolved in 3 mL of distilled water in a quantity to achieve a potential maximum concentration of Biotin T ® at 0.5 % in the solution.

UV–visible spectroscopy analyses were conducted using an Agilent Technologies Cary300 UV–vis spectrophotometer. The analyses were run through the Cary WinUV Scan software 4.20. The absorbance peak around 250–300 nm of the OIT molecule was used as a reference for the presence of Biotin T ®.

The study has been conducted in triplicate with a error lower than 5 %.

All data sets were processed with the software Origin 2021 by OriginLab, Northampton, MA, USA.

3. Results and discussion

The selection of MCM-41 as silica nanocontainer was based on the size of Biotin T ® molecules (~1 nm) and the diameters of the nanopores; which are approximately 3 nm for MCM-41 and broader for other kinds of ordered mesoporous silica [48,49]. Therefore, the study was centered on nanomaterials with smaller pores, to effectively hold and interact with the commercial biocide. The surface of silica can be modified ad hoc to tune the interaction with the host molecules didecyldimethylammonium chloride (DDAC) and 2-octyl-2 H-isothiazol-3-one (OIT).

Table 1
Inhibition area of Biotin T ® in different concentrations over *Cladosporium* sp. Fungi.

Sample	Inhibition Area (cm^2)	Standard Deviation (SD)
Negative control	0	± 0
0.1 %	30	± 5
0.3 %	77	± 6
1 %	185	± 6
3 %	304	± 6
10 %	(max)	± 0
30 %	(max)	± 0

3.1. Biotin T ® activity microbiological test

The microbiological test was conducted to obtain preliminary information regarding the biocidal efficacy of various concentrations of Biotin T ® solutions, with the aim of understanding the amount of impregnated silica NPs needed to ensure effective antimicrobial action revisiting the principles of the Kirby-Bauer Diffusion-Test Method (*i.e.* the antimicrobial diffuses from the disk into the agar and the fungal growth is inhibited at a distance from the disk that is proportional to its specific susceptibility).

From the photos taken after 7 days from inoculation, as illustrated in Fig. 2, it is evident that the inhibition area – *i.e.*, the area where the growth of *Cladosporium* sp. Fungi is not observed – increases with the concentrations of Biotin T ® solutions. The picture of the negative control is also provided for comparison (Fig. 2a). These solutions demonstrate low effectiveness at concentrations ≥ 0.1 % (Fig. 2b); when the concentration exceeds 1 % (Fig. 2d), there is no observable fungal growth (complete inhibition), *i.e.* no spore germination and/or mycelium growth and proliferation all around (radially) the Biotin T ® impregnated paper discs.

Table 1 reports data on the inhibition areas of the samples; the result obtained for each sample corresponds to the average of the results from the three cellulose disks impregnated with Biotin T ® within the three Petri dishes. For the concentrations at 10 % and 30 %, it is reported the whole area of the Petri dish, since growth was not identified.

Regarding the negative control, the inhibition area corresponds to 0, as the Fungi completely cover the Petri dishes, including the cellulose

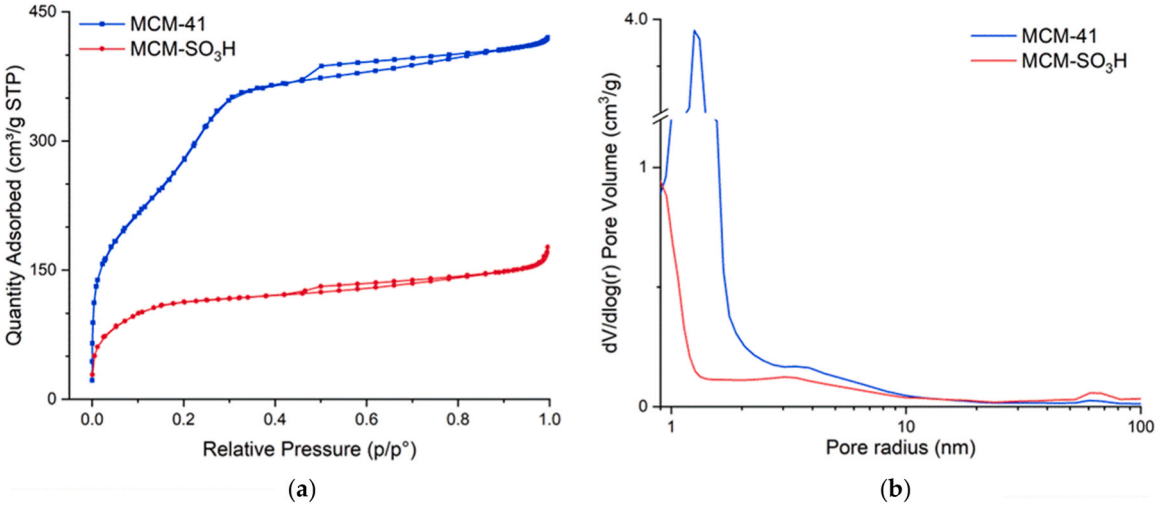

Fig. 3. N_2 physisorption graphs of MCM-41 (in blue) and MCM-SO_3H (in red): (**a**) Hysteresis graphs; (**b**) Chart depicting the pore volume as a function of pore size distribution.

disks. With the 0.1 % sample, the average inhibition area is lower than that of the cellulose disk impregnated with Biotin T ® (~18 cm^2); indeed, the Fungi were able to colonize part of the cellulose disks. From the 0.3 % (Fig. 2c) concentration onward, a notably higher inhibition area is observed, increasing further with 1 %, concentration at which complete radial inhibition is observed (Fig. 2d) with subsequent confluent growth. This result is confirmed with the 3 % sample (Fig. 2e) and reaching total inhibition on the overall Petri area with the 10 % and 30 % samples (Fig. 2f and 2 g).

These results indicate that the biocide is effective even at low concentrations. Therefore, in the case of gradual release, the minimum concentration necessary to exert antimicrobial action can be easily achieved.

3.2. Characterizations of the silica matrices

The central part of the study was focused on the characterization of both MCM-41 and the functionalized silica matrix MCM-SO_3H, also focusing on the intermediate step MCM-SH. Their different structure and features are indeed closely related to their delivery performances. Furthermore, some analyses were carried out on the impregnated samples with Biotin T ® (MCM-41-BT and MCM-SO_3H-BT).

3.2.1. N_2 physisorption

The analysis was employed to evaluate the surface characteristics of the materials. As shown in Fig. 3a, both analyzed samples exhibit a Type IV isotherm, indicative of MCM-41 typical hysteresis. It is noticeable that, at the same relative pressure (p/p°), the amount of N_2 absorbed in the MCM-41 pores is higher than that absorbed by the MCM-SO_3H ones. This suggests a successful grafting procedure: the loss in volume and surface area could be due to the covalently bonded functional groups that partially occupy the material's pores, as confirmed by the BJH curve, shown in Fig. 3b. MCM-41 presents a BET surface area of 920 m^2/g and a BJH cumulative pore volume of 0.750 cm^3/g. After the grafting procedure, these values significantly decrease, resulting in a BET surface area of 413 m^2/g and a BJH cumulative pore volume of 0.205 cm^3/g for MCM-SO_3H.

Concerning the pore size of the two materials, the analysis reveals that the average pore diameter for both samples is approximately 3 nm. However, it can be observed that in the case of MCM-SO_3H the hysteresis begins to form at slightly lower pressures compared to the MCM-41. This suggests a more heterogeneous distribution of pore sizes in the material (Fig. 3b). It is therefore possible that the grafting treatment might have partially altered the material's structure. To further investigate the influence of the grafting procedure on the structure of the silica matrices, X-ray diffraction measurements were also performed.

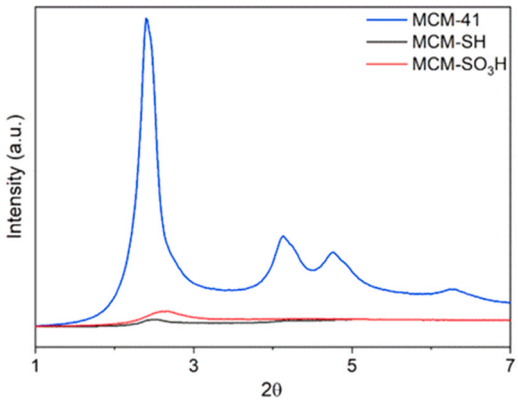

Fig. 4. X-ray diffraction graph of three samples: MCM-41 (in blue), MCM-SH (in black), and MCM-SO_3H (in red).

3.2.2. X-ray diffraction (XRD)

In Fig. 4a significant loss of the long-range order can be observed due to the action of the grafting treatment on the porous structure of MCM-41. This is shown by a drastic intensity reduction of the main peak and the disappearance of secondary peaks in the MCM-SO_3H profile.

Furthermore, in comparison to the initial d-spacing of 36.8 Å, there is an initial contraction in the MCM-SH structure, reducing the d-spacing to 35.0 Å, followed by a second contraction in MCM-SO_3H, which has a d-spacing of 33.5 Å.

3.2.3. Analysis of the acid sites by back-titrations

The effectiveness of the grafting procedure was verified through a synergy of approaches. The first involved a preliminary analysis to roughly assess the sulfonic group grafted on the sample: a back-titration test was conducted, as it represents a quick and straightforward investigation method: 50 mg of MCM-41 were titrated with 1.35 mL of HCl, corresponding to 0.27 $\bullet 10^{-4}$ mol of acid. Using the relationship (1):

$$\text{moles of NaOH} - \text{acid groups moles} = \text{moles of HCl}, \quad (1)$$

it was possible to determine the number of moles of acidic groups in the material that reacted with NaOH, namely 1.73 $\bullet 10^{-4}$ mol.

As for the back-titration of MCM-SO_3H, 1.05 mL of HCl was required,

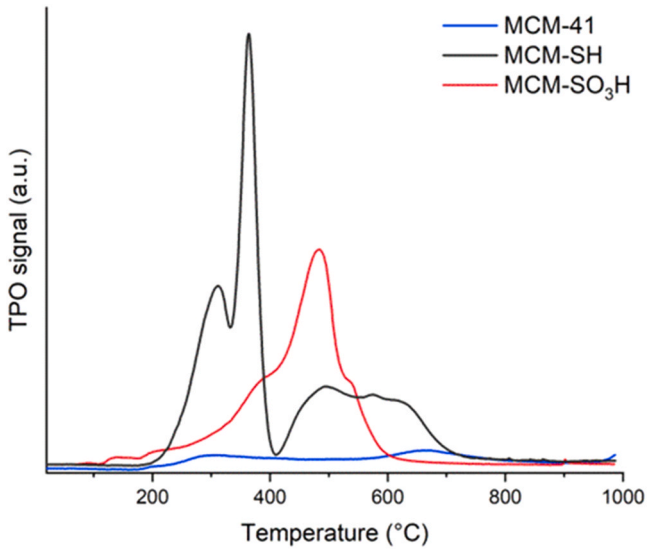

Fig. 5. TPO graph of MCM-41 samples (in blue), MCM-SH (in black), and MCM-SO_3H (in red).

equivalent to 0.21 •10^{-4} mol. Using the same relationship (1), the moles of acidic groups that reacted were 1.79 •10^{-4} mol.

Comparing the two results, it is noticeable that in the case of the basic solution containing MCM-41 a lower number of acidic groups reacted with NaOH. This could be attributed to the lower acidity of the –OH groups present on the surface of MCM-41, compared to the –SO_3H groups added after grafting.

3.2.4. *Temperature Programmed Oxidation (TPO)*

The Temperature-Programmed Oxidation (TPO) technique was employed to determine, based on the increasing temperature and consumption of the oxidizing mixture, the presence of oxidizable species in the analyzed samples. In the graph reported in Fig. 5, it can be observed that the three matrices exhibit very different behaviors as the temperature increases. In detail, the MCM-41 curve does not show significant peaks, unlike MCM-SH and MCM-SO_3H; this aspect can be attributed to the decomposition of chemical species.

Regarding the other two samples, hypotheses can be made by referring to what is present in the literature [50]. In the curve of MCM-SH, a very intense peak is noticeable just before 400 °C; it can be attributed to the oxidation of the –SH groups linked to the silica surface. The broadband after 400 °C is probably due to the overlapping of different processes involving different species present in the sample. Two shoulders are recognizable in the band: the first, at around 500 °C, could be due to the decomposition of the sulfonic groups formed after the oxidation of thiols, while the second at 550 – 600 °C may be due to the decomposition of the alkyl chain directly bonded to the silica [50].

These hypotheses can be supported by the analysis of MCM-SO_3H, whose curve shows an intense peak at around 500 °C, which can be attributed to the decomposition of propyl-sulfonic groups linked to the material. The curve also exhibits two shoulders that develop at temperatures comparable to the peaks in the MCM-SH profile. The first, around 400 °C, is probably due to the oxidation of –SH groups that were not completely oxidized during the H_2O_2 procedure and have lower intensity compared to those present in the MCM-SH profile. The second shoulder, at around 550 °C, is associated with the decomposition of alkyl chains bonded to the material.

To support and complement the information obtained from the TPO analysis, Thermogravimetric (TG) and Differential Thermal Analysis (DTA) were performed and are discussed in the following section.

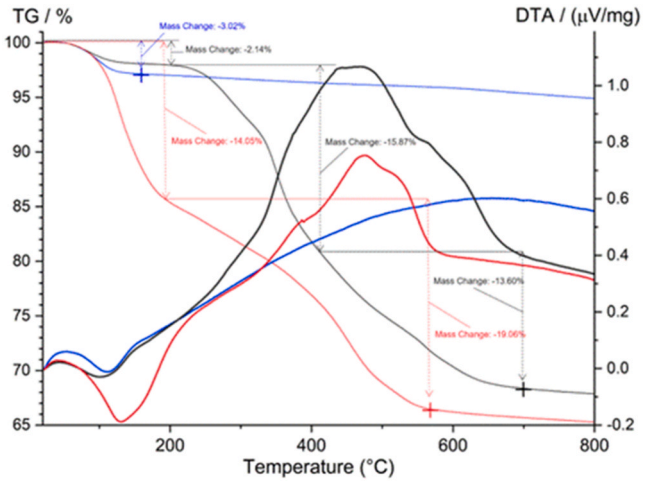

Fig. 6. Graph depicting TG and DTA analyses of three different samples: MCM-41 (in blue), MCM-SH (in black), and MCM-SO_3H (in red).

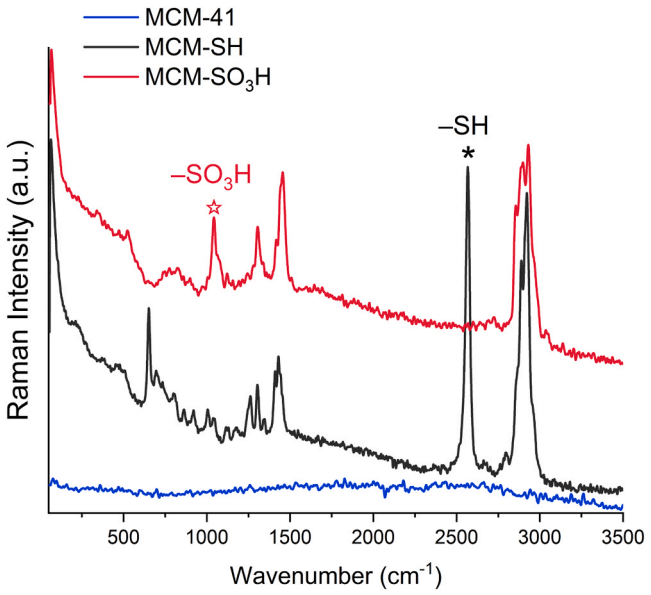

Fig. 7. Raman spectra of three samples: MCM-41 (in blue), MCM-SH (in black), and MCM-SO_3H (in red).

3.2.5. *Thermal analyses (TG/DTA)*

Thermogravimetric analysis (TG) and Differential Thermal Analysis (DTA) (in Fig. 6) allowed the evaluation of the mass losses (%) of the three different samples as the temperature increased. These losses were associated with exothermic or endothermic processes leading to the degradation of chemical species.

In the TG analysis, in all three samples, a first weight loss up to 200 °C is noticeable: it could be associated with the evaporation of interstitial H_2O present in the pores of the materials. In the case of the MCM-41, this is the only percentage loss recorded. These weight losses are reflected in the DTA, where endothermic processes are evident up to 150 °C, likely they were needed to provide the necessary energy for water to evaporate from the material's pores. In the case of the MCM-SO_3H, the weight loss is higher than the others, probably because it contained a greater amount of H_2O; this is justified by the DTA analysis in which the associated endothermic process peak is more pronounced than those of the other two samples.

In the MCM-SH TG analysis, a second weight loss between 200 °C and 400 °C was attributed to the decomposition of –SH groups, followed

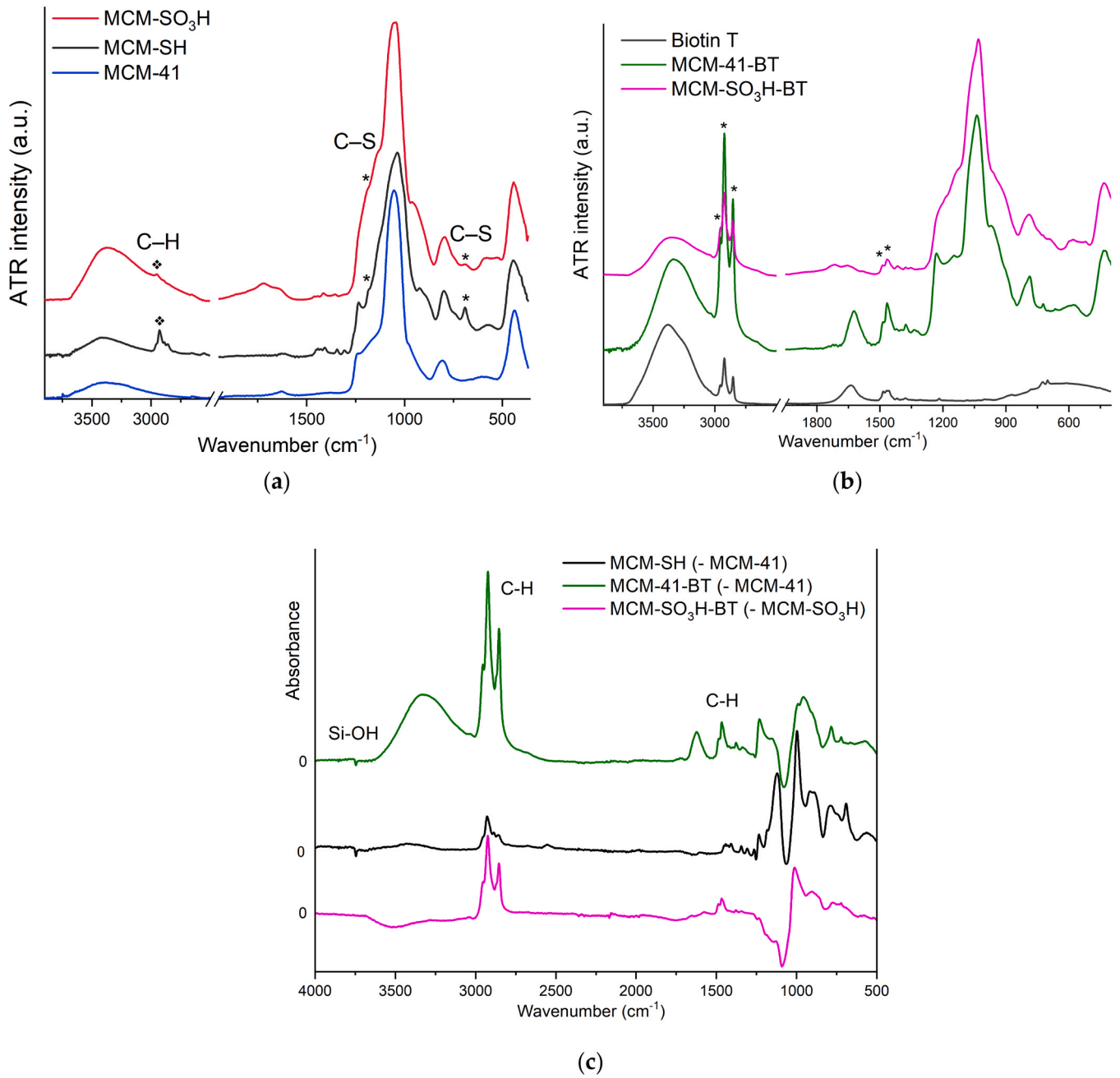

Fig. 8. (**a**) ATR spectra of three samples: MCM-41 (in blue), MCM-SH (in black), MCM-SO_3H (in red); (**b**) ATR spectra of the impregnated samples MCM-41-BT (in green) and MCM-SO_3H-BT (in pink) compared with the ATR spectra of Biotin T ® (in black) with highlighted the Biotin T ® related signal; (**c**) Differential spectra of the samples MCM-SH (in black) and of the impregnated sample MCM-41-BT (in green) and MCM-SO_3H-BT (in pink).

by a third weight loss, up to 700 °C, which was attributed to the decomposition of the alkyl chains linked to them. In the DTA analysis, it is possible to observe the development of exothermic processes in the temperature range of 100–700°C, ascribed to the decomposition of these chemical species.

Regarding MCM-SO_3H, the second significant weight loss in the DTA, approximately between 200 °C and 600 °C, is associated with exothermic processes that could have involved the decomposition of various species, such as the –SH groups that were not oxidized during grafting, –SO_3H groups, and the alkyl chains bonded to the silica.

3.2.6. *Raman spectroscopy*

Through Raman and ATR spectroscopic analyses the surface properties of the silica matrices, before and after grafting, as well as the functional groups contained in them, were studied.

Regarding Raman spectroscopy, in the graph shown in Fig. 7, it can be observed that, while MCM-41 exhibits almost no detectable vibrations, the spectrum of MCM-SH shows a very intense signal at 2570 cm^{-1} attributable to the presence of thiol groups (–SH). This signal disappears following oxidation in MCM-SO_3H, revealing the signal of sulfonic groups (–SO_3H) at around 1050 cm^{-1}.

3.2.7. *Attenuated Total Reflectance (ATR) infra-red spectroscopy*

ATR spectrum of MCM-41 presents the characteristic band of silica, in particular an intense and broad band centered at 1060 cm^{-1} related to the asymmetric stretching O–Si–O units, and other weaker signals at ~800 and 410 cm^{-1} attributable to symmetric stretching and bending modes of O–Si–O.

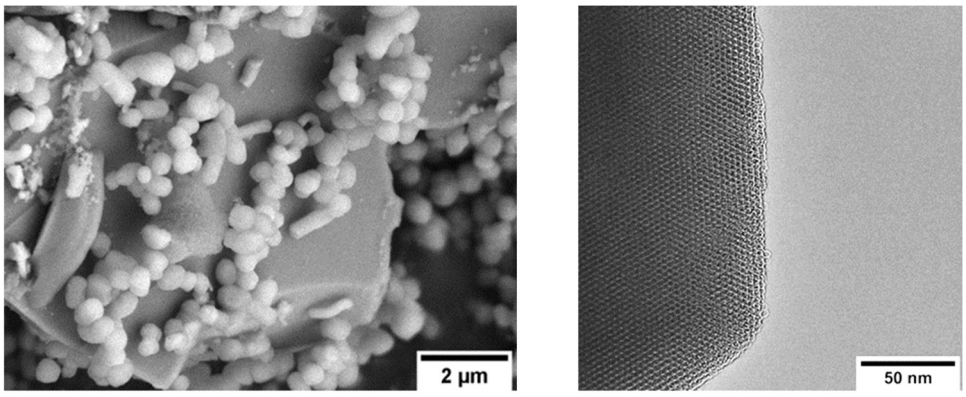

(a) (b)

Fig. 9. (**a**) SEM micrograph of the sample MCM-41; (**b**) HRTEM micrographs of the sample MCM-41: the view of the material along the hexagonal axis.

In the ATR spectrum of MCM-SH (in Fig. 8a) there is a signal at around 2900 cm^{-1} attributable to the C–H stretching of the aliphatic chains bonded to the material's surface. This signal becomes weaker and undefined after oxidation, also due to the presence of a larger amount of water, if compared to the other two samples. After grafting, in MCM-SH and MCM-SO_3H, two additional signals at 1240 cm^{-1} and 690 cm^{-1} are singled out, respectively attributable to the C–S vibrations of the functional groups.

In the spectrum of commercial Biotin T ® (50 % in water solution) only the signals of aliphatic chains, present in both DDAC and OIT molecules, are recognizable. The intense stretching mode of methyl and methylen groups below 3000 cm^{-1} and corresponding bending modes around 1460 cm^{-1} are evident in samples containing Biotin T ®, MCM-41-BT, and MCM-SO_3H-BT, confirming the effectiveness of the impregnation method (Fig. 8b).

Differential spectra were obtained (in Fig. 8c), trying to do some consideration on the nature of interaction between surface and impregned molecules. For MCM-41-BT we observed that impregnation consume the signal of isolated surface silanol, so we can suppose that for plain MCM-41 the impregnation mechanism involved, almost in part, the formation of H bond between isolated Si-OH and carbonyl of OIT. MCM-SO_3H does not present free silanols, that were involved in grafting with MPTMS, and impregnation seems to consume part of H-bonding. For sample containing Biotin T ® differential spectra evidence also modification of silica modes, probably related to a slight modification of material network. No consideration can be done on sulfonate groups, which signals are superimposed to intense silica mode.

3.2.8. Scanning Electron Microscopy (SEM) and High-Resolution Transmission Electron Microscopy (HRTEM)

The electron microscopy techniques (*i.e.*, SEM and TEM) were employed to study the morphology and topography of the silica matrices. Fig. 9 reports both SEM and TEM images referred to the MCM-41 mesoporous silica matrix. The SEM micrograph (section a) shows that the nanoparticles possess a spherical shape with an average size of around 500 nm. From the HRTEM micrograph (section b) it can be seen that this material has the characteristic short-range-ordered mesoporous structure of hexagonal symmetry with alternating channels and siliceous network. The pore width, as determined from HRTEM micrographs is approximately 3 nm.

For MCM-SO_3H, the SEM micrographs were coupled with an Energy-Dispersive X-ray Spectroscopy (EDS) analysis. Fig. 10 reports the SEM micrograph of the sample (a) and the Map Sum Spectrum (b) confirming the presence of sulfur (S), besides oxygen (O) and silicon (Si); from the elemental mapping it can be noticed that S (e) is as homogeneously distributed as Si (c) and O (d); this suggests a correct dispersion of the grafting treatment along the material.

Moreover, from the HRTEM micrograph (Fig. 10 – f) both the hexagonal structure, also present in MCM-41, and the view perpendicular to the hexagonal axis can be identified. This characterization confirms that, even though the material underwent modification, the fundamental original structure has been preserved.

The SEM micrographs of sample MCM-41-BT were coupled with an EDS analysis as well. Fig. 10 reports the SEM micrograph of the sample (a) and the total map sum spectrum (b) confirming the presence of chlorine (Cl), besides O and Si. From the elemental mapping, it can be noticed that chlorine is well distributed as Si (c) and O (d); this suggests a homogeneity in the impregnation treatment.

From the HRTEM micrograph (Fig. 11 – f) the characteristic MCM-41 structure can be identified, from the view perpendicular to the hexagonal axis. This characterization confirms that the fundamental original structure has been once again preserved.

Fig. 12 shows the SEM (a), along with an EDS analysis (b-e), and the TEM (f) micrographs of sample MCM-SO3H-BT. From the elemental mapping, it is possible to see, besides Si (c) and O (d), the homogeneous distribution of S (e). In this case, the presence of Cl was not detected, probably due to its low amount in the sample: considering that Biotin T ® concentration in the matrix is 0.5 mL/g and that the DDAC molecule, containing Cl, is generally present at 40–60 % in the product, the amount of DDAC in the analyzed sample would be around 0.2–0.3 %. Furthermore, the low elemental amount of Cl in the molecule must be considered. Therefore, it could be stated that the low amount of Cl is the main responsible for its absence in the EDS map.

From the HRTEM micrograph (Fig. 12 – f) the characteristic MCM-41 particle shape can be identified, suggesting that the fundamental original structure has been once again preserved. It is worth mentioning that in both impregnated samples, MCM-41-BT and MCM-SO_3H-BT, the organic compounds of Biotin T ® cause interference, making the sample beam sensitive, and thus resulting in less defined HRTEM images. It was however possible to identify the material characteristic planes, which appear as pale parallel lines in the micrographs.

In summary, from SEM, EDS, and TEM analyses it was possible to highlight that the functionalized silica matrix MCM-SO_3H does not differ in structure from the original MCM-41. Additionally, the –SO_3H groups, identified through the S element, were successfully homogeneously distributed over the material. For what concerns the impregnated matrices MCM-41-BT and MCM-SO_3H-BT, it was possible to notice the presence of Cl, representing the antimicrobial product Biotin T ®, that is didecyldimethylammonium chloride (DDAC) molecules.

3.3. Study of the release systems

After studying the properties of the silica nanocontainers, their performance was assessed through in vitro release tests to verify their

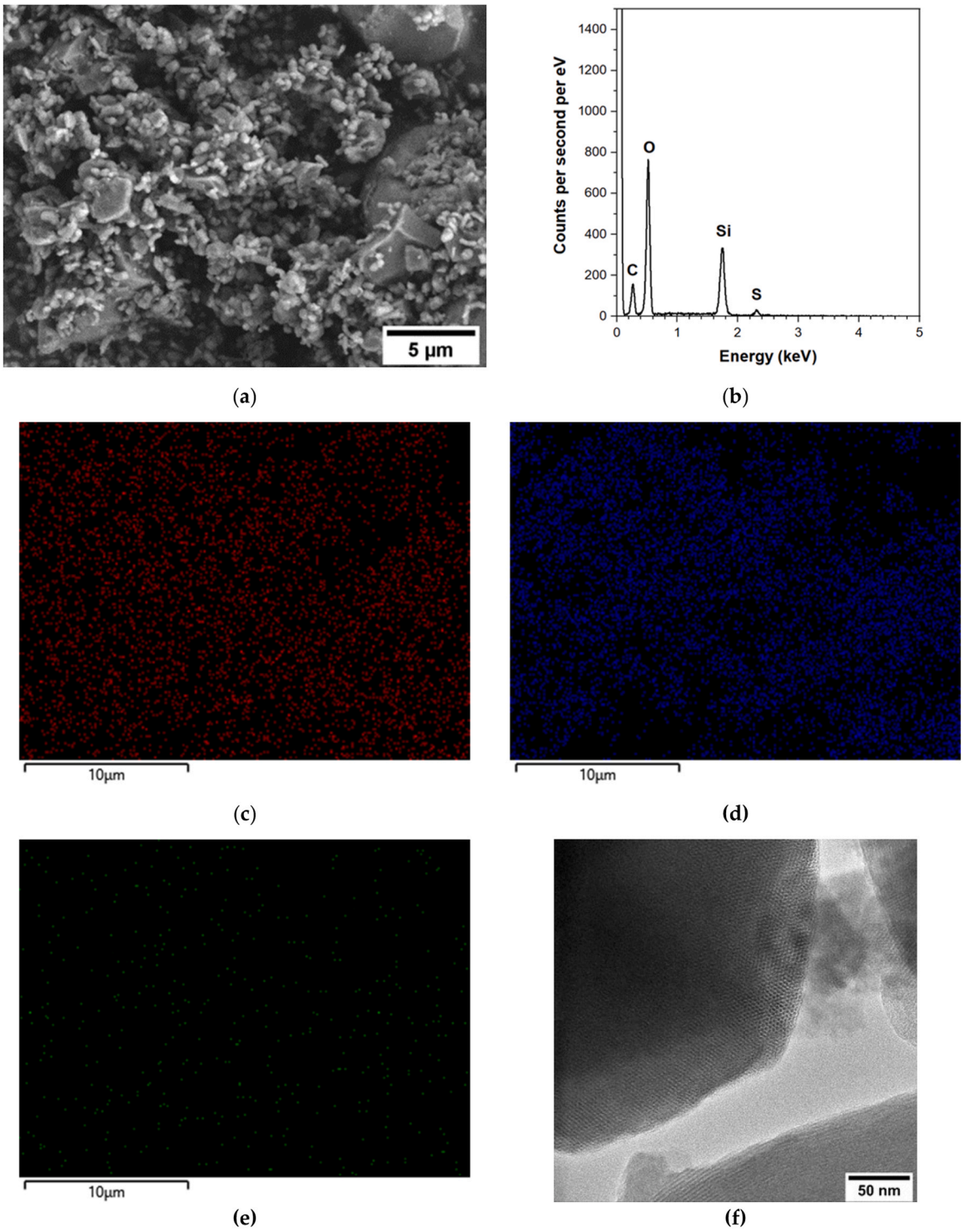

Fig. 10. (**a**) SEM micrograph of the sample MCM-SO_3H; (**b**) total EDS map sum spectrum; (**c**) EDS elemental mapping of Si; (**d**) EDS elemental mapping of O; (**e**) EDS elemental mapping of S; (**f**) TEM micrograph of the sample MCM-SO_3H, showing the view both along (top) and perpendicular (bottom) to the hexagonal axis.

capacity to deliver the biocide product.

From UV–visible analysis, it was possible to determine, through the absorbance values of the molecule 2-octyl-2 H-isothiazol-3-one (OIT), the concentration of Biotin T ® present in the various solutions at specific intervals over time, allowing for the evaluation of the effectiveness of the MCM-41 and MCM-SO_3H matrices.

From the graph in Fig. 8a, it can be observed that with MCM-41 the biocide is rapidly released into the solution with a percentage of ~22 % within the first hour, maintaining a constant concentration for 15 days (360 hours).

On the other hand, with MCM-SO_3H, the concentration of Biotin T ® in the solution progressively increases over time, reaching ~38 % after 15 days (360 hours). For this sample it was also carried out a 30-day sample: in this case, the concentration further increased to 46 %. Thus, OIT is released in greater quantity and more gradually from MCM-SO_3H compared to MCM-41, where, after a certain threshold the OIT concentration does not increase further but remains constant.

Since a controlled release system is influenced by various factors,

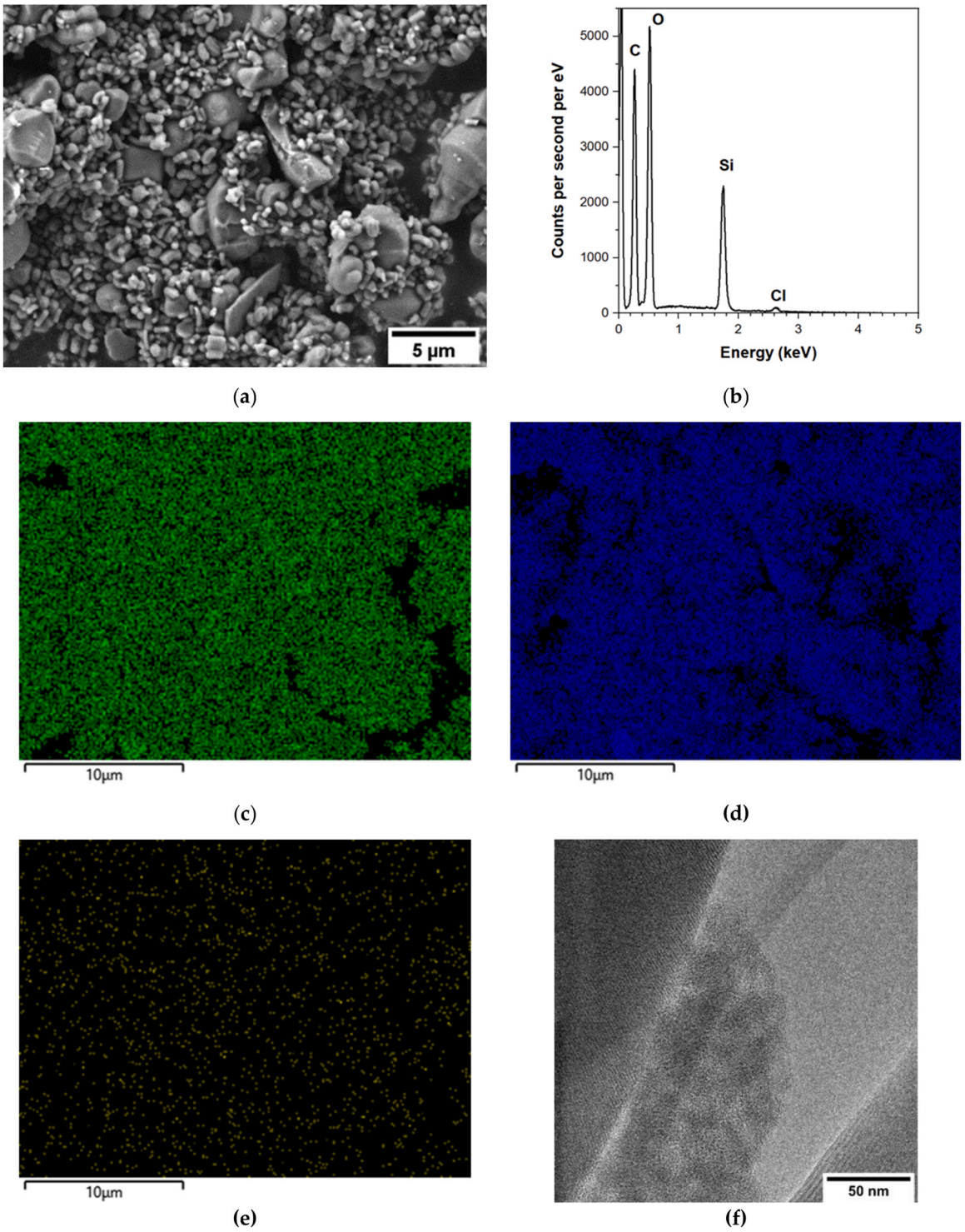

Fig. 11. (**a**) SEM micrograph of the sample MCM-41-BT; (**b**) EDS map sum spectrum; (**c**) EDS elemental mapping of Si; (**d**) EDS elemental mapping of O; (**e**) EDS elemental mapping of Cl; (**f**) TEM micrograph of the sample MCM-41-BT.

including pores size and shape and the chemical-physical interactions that can occur between the matrix and the active component, it is possible to hypothesize that MCM-SO_3H offers a less ordered structure that favors the release of a greater quantity of biocide compared to MCM-41 (Fig. 13 b, c). The porosity of the modified sample, which appears more heterogeneous with a certain percentage of smaller pores compared to those of the unmodified sample, probably explains the slower release kinetics in the initial phase. The less ordered porous structure, while controlling release, facilitates the diffusion of a greater amount of the active compound. Additionally, the release is influenced by the different nature of the nanocapsules: the weak interaction with the sulfonate surface groups also promotes gradual release. They could interact through a hydrogen bond that may form between the hydrogen atom attached to the sulfonic groups and the numerous nonbonding electron pairs present on the ring of the OIT molecule. Another boost to the release is the increased affinity with the release medium, which in this case is aqueous. The surface of MCM-SO_3H is certainly more compatible with the medium and therefore likely promotes the release

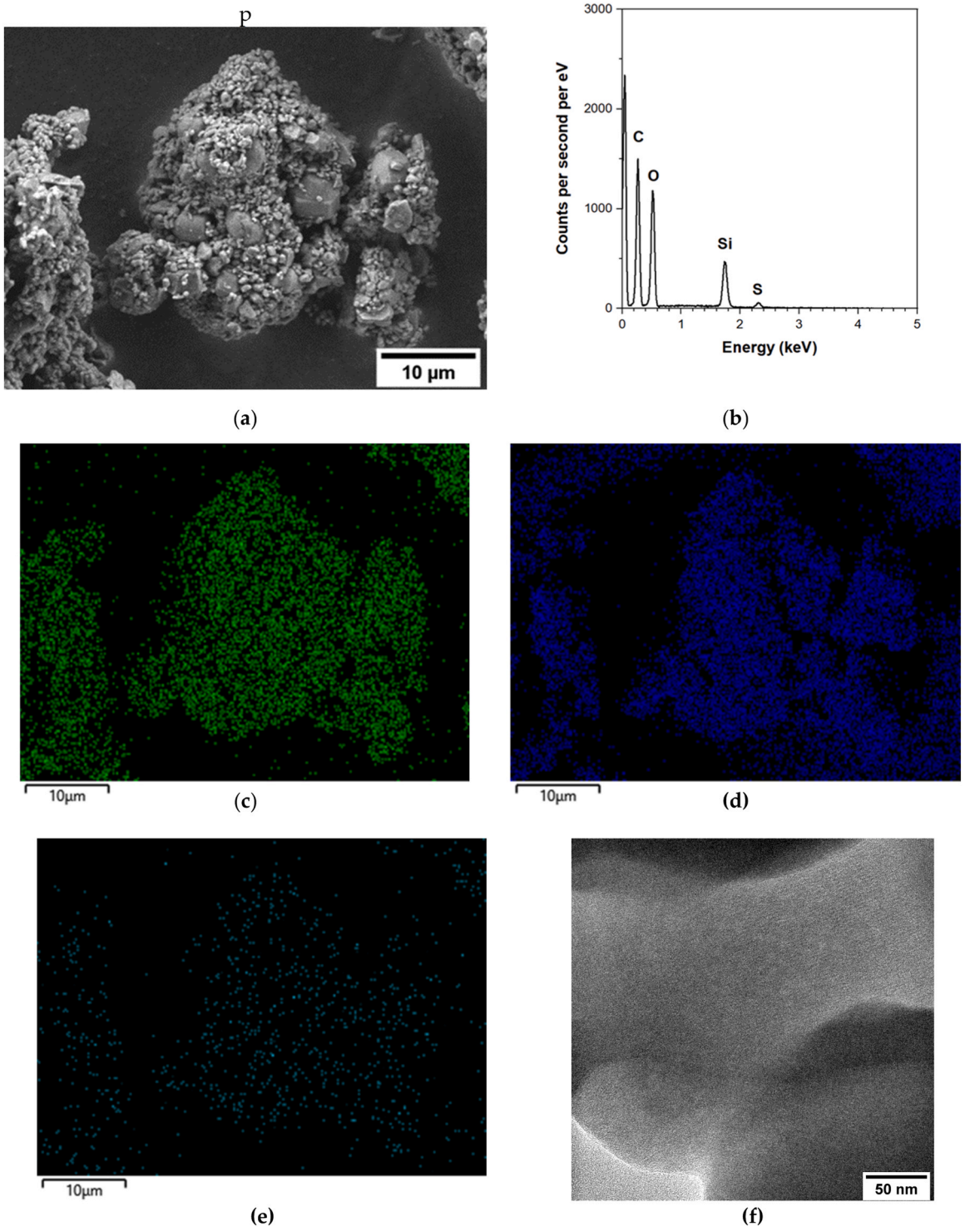

Fig. 12. (**a**) SEM image of the sample MCM-SO_3H-BT; (**b**) EDS map sum spectrum; (**c**) EDS elemental mapping of Si; (**d**) EDS elemental mapping of O; (**e**) EDS elemental mapping of S; (**f**) TEM image of the sample MCM-SO_3H-BT.

of a greater quantity of the active ingredient.

Regarding the determination of the DDAC molecule, although it was not possible to quantify its concentration in the solution, the UV–visible absorbance spectra show a progressive increase in the absorption band intensity over time in the MCM-SO_3H sample, which could justify a gradual release of the molecule from the matrix pores.

4. Conclusions

Within this work, a multifunctional silica NP-based matrix was successfully synthesized and functionalized that, due to its characteristics, allows the encapsulation and a gradual release of the commercial biocidal product Biotin T ®, commonly employed in the stone restoration field. The material is aimed to be suspended into a polymeric-based formulation as the principal component of an antimicrobial protective coating for stone surfaces. This work aims indeed to limit or prevent the

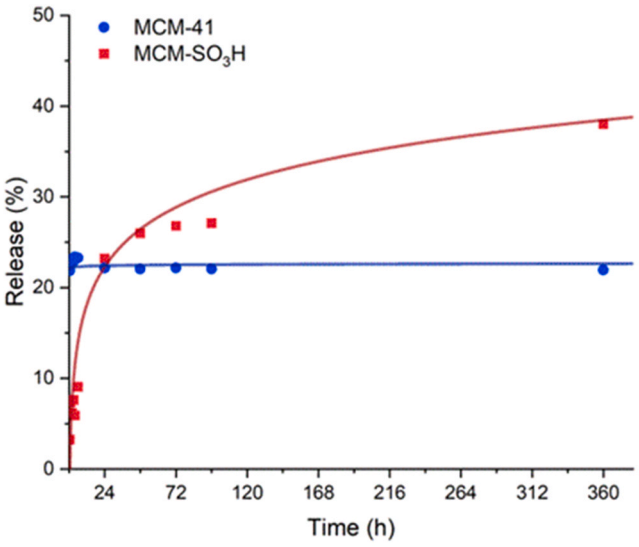

(a)

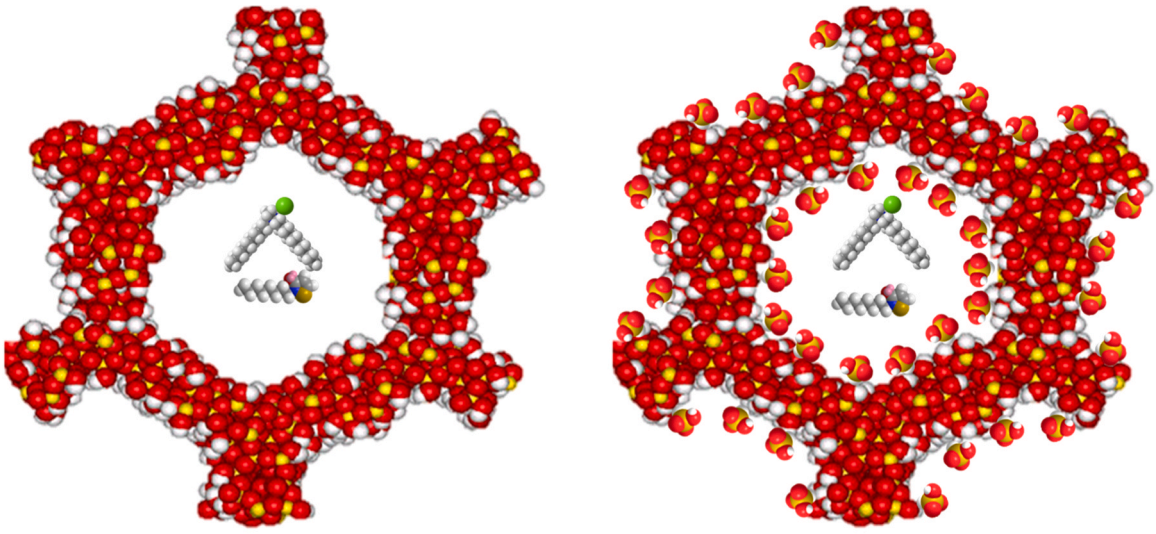

(b) (c)

Fig. 13. (a) The concentration of Biotin T ® in aqueous solution over time; (b) 3D representation of the MCM-41 structure containing the two molecules composing Biotin T ®; (c) 3D representation of the MCM-SO_3H structure containing the two molecules composing Biotin T ®.

growth of microorganism colonies on stone surfaces, preserving them from biodeterioration phenomena and minimizing the need for cleaning interventions. Additionally, the proposed approach is not only environmentally greener but also more sustainable for the health of the operators and economically.

CRediT authorship contribution statement

Andrea Campostrini: Formal analysis, Conceptualization, Data curation, Writing – original draft, Preparation, Visualization. Elena Ghedini: Conceptualization, Validation, Methodology, Writing – review & editing. Teresa Botrè: Formal analysis, Visualization. Sabrina Manente: Formal analysis. Alessia Giordana: Formal analysis, Investigation. Giuseppina Cerrato: Writing – review & editing. Giuseppe Cruciani: Formal analysis. Alex W. Robertson: Formal analysis, Writing – review & editing Michela Signoretto: Resources, Supervision, Writing – review & editing. Federica Menegazzo**:** Resources, Conceptualization, Supervision, Writing – review & editing.

Declaration of Competing Interest

The authors declare no competing interest.

Acknowledgments

The authors would like to acknowledge Mr. Nicola Calderaro and Ms. Tania Fantinel for their practical contributions to this work. Andrea Campostrini finally would like to thank the “PON Ricerca e Innovazione 2014–2020”, “Fondo per la promozione e lo sviluppo delle politiche del Programma Nazionale per la Ricerca (PNR) 2021–2027”, and the restoration company Uni.S.Ve. S.r.l. of Venice (Italy) for financing his Ph.D. scholarship.

References

[1] F. Sbardella, M.P. Bracciale, M.L. Santarelli, J.M. Asua, Waterborne modified-silica/acrylates hybrid nanocomposites as surface protective coatings for stone monuments, Prog. Org. Coat. 149 (2020) 105897, https://doi.org/10.1016/j.porgcoat.2020.105897.

[2] D. De la Fuente, J.M. Vega, F. Viejo, I. Díaz, M. Morcillo, Mapping air pollution effects on atmospheric degradation of cultural heritage, J. Cult. Herit. 14 (2013) 138–145, https://doi.org/10.1016/J.CULHER.2012.05.002.

[3] L. Canesi, A. Sardella, R. Vogler, A. Kaiser, C. Vaccaro, A. Bonazza, Hazard analysis and vulnerability assessment of cultural landscapes exposed to climate change-related extreme events: a case study of wachau (Austria), Heritage 7 (2024) 1917–1934, https://doi.org/10.3390/heritage7040091.

[4] T. Warscheid, J. Braams, Biodeterioration of stone: a review, Int Biodeterior. Biodegrad. 46 (2000) 343–368, https://doi.org/10.1016/S0964-8305(00)00109-8.

[5] A. Michaelsen, F. Pinzari, N. Barbabietola, G. Piñar, Monitoring the effects of different conservation treatments on paper-infecting fungi, Int Biodeterior. Biodegrad. 84 (2013) 333–341, https://doi.org/10.1016/j.ibiod.2012.08.005.

[6] L. Schröer, N. Boon, T. De Kock, V. Cnudde, The capabilities of bacteria and archaea to alter natural building stones – a review, Int Biodeterior. Biodegrad. 165 (2021) 105329, https://doi.org/10.1016/J.IBIOD.2021.105329.

[7] J. Becerra, M. Mateo, P. Ortiz, G. Nicolás, A.P. Zaderenko, Evaluation of the applicability of nano-biocide treatments on limestones used in cultural heritage, J. Cult. Herit. 38 (2019) 126–135, https://doi.org/10.1016/j.culher.2019.02.010.

[8] I.A. Jones, L.T. Joshi, Biocide use in the antimicrobial era: a review, Molecules 26 (2021) 2276, https://doi.org/10.3390/molecules26082276.

[9] E. Kampasakali, T. Fardi, E. Pavlidou, D. Christofilos, Towards sustainable museum conservation practices: a study on the surface cleaning of contemporary art and design objects with the use of biodegradable agents, Heritage 4 (2021) 2023–2043, https://doi.org/10.3390/heritage4030115.

[10] A.J. Fonseca, F. Pina, M.F. Macedo, N. Leal, A. Romanowska-Deskins, L. Laiz, A. Gómez-Bolea, C. Saiz-Jimenez, Anatase as an alternative application for preventing biodeterioration of mortars: evaluation and comparison with other biocides, Int Biodeterior. Biodegrad. 64 (2010) 388–396, https://doi.org/10.1016/j.ibiod.2010.04.006.

[11] C. Dresler, M.L. Saladino, C. Demirbag, E. Caponetti, D.F. Chillura Martino, R. Alduina, Development of controlled release systems of biocides for the conservation of cultural heritage, Int Biodeterior. Biodegrad. 125 (2017) 150–156, https://doi.org/10.1016/j.ibiod.2017.09.007.

[12] T. Yoshimatsu, K.-I. Hiyama, Mechanism of the Action of Didecyldimethylammonium chloride (DDAC) against Escherichia coli and Morphological Changes of the Cells, Biocontrol Sci. 12 (2007) 93–99, https://doi.org/10.4265/bio.12.93.

[13] V. Silva, C. Silva, P. Soares, E.M. Garrido, F. Borges, J. Garrido, Isothiazolinone biocides: chemistry, biological, and toxicity profiles, Molecules 25 (2020) 991, https://doi.org/10.3390/molecules25040991.

[14] J.O. Morley, A.J. Oliver Kapur, M.H. Charlton, Structure–activity relationships in 3-isothiazolones, Org. Biomol. Chem. 3 (2005) 3713, https://doi.org/10.1039/b509529h.

[15] A. Artesani, F. Di Turo, M. Zucchelli, A. Traviglia, Recent advances in protective coatings for cultural heritage–an overview, Coatings 10 (2020) 217, https://doi.org/10.3390/coatings10030217.

[16] V. Gomes, A. Dionísio, J.S. Pozo-Antonio, Conservation strategies against graffiti vandalism on Cultural Heritage stones: Protective coatings and cleaning methods, Prog. Org. Coat. 113 (2017) 90–109, https://doi.org/10.1016/J.PORGCOAT.2017.08.010.

[17] M. Frigione, M. Lettieri, Novel attribute of organic–inorganic hybrid coatings for protection and preservation of materials (stone and wood) belonging to cultural heritage, Coatings 8 (2018) 319, https://doi.org/10.3390/coatings8090319.

[18] S.A. Ruffolo, M.F. La Russa, M. Malagodi, C. Oliviero Rossi, A.M. Palermo, G. M. Crisci, ZnO and ZnTiO3 nanopowders for antimicrobial stone coating, Appl. Phys. A 100 (2010) 829–834, https://doi.org/10.1007/s00339-010-5658-4.

[19] S.A. Ruffolo, M.F. La Russa, Nanostructured coatings for stone protection: an overview, Front Mater. 6 (2019), https://doi.org/10.3389/fmats.2019.00147.

[20] M. Roveri, F. Gherardi, S. Goidanich, D. Gulotta, V. Castelvetro, R. Fischer, L. Winandy, J. Weber, L. Toniolo, Self-cleaning and antifouling nanocomposites for stone protection: properties and performances of stone-nanomaterial systems, IOP Conf. Ser. Mater. Sci. Eng. 364 (2018) 012070, https://doi.org/10.1088/1757-899X/364/1/012070.

[21] R. Lamuraglia, A. Campostrini, E. Ghedini, A. De Lorenzi Pezzolo, A. Di Michele, G. Franceschin, F. Menegazzo, M. Signoretto, A. Traviglia, A new green coating for the protection of frescoes: from the synthesis to the performances evaluation, Coatings 13 (2023) 277, https://doi.org/10.3390/coatings13020277.

[22] F. Gherardi, P.N. Maravelaki, Advances in the application of nanomaterials for natural stone conservation, RILEM Tech. Lett. 7 (2022) 20–29, https://doi.org/10.21809/rilemtechlett.2022.159.

[23] P. Baglioni, E. Carretti, D. Chelazzi, Nanomaterials in art conservation, Nat. Nanotechnol. 10 (2015) 287–290, https://doi.org/10.1038/nnano.2015.38.

[24] T.A. Debele, S.L. Mekuria, H.-C. Tsai, Polysaccharide based nanogels in the drug delivery system: application as the carrier of pharmaceutical agents, Mater. Sci. Eng.: C. 68 (2016) 964–981, https://doi.org/10.1016/j.msec.2016.05.121.

[25] P. Severino, J.F. Fangueiro, M.V. Chaud, J. Cordeiro, A.M. Silva, E.B. Souto, Advances in nanobiomaterials for topical administrations: new galenic and cosmetic formulations. in: Nanobiomaterials in Galenic Formulations and Cosmetics, Elsevier, 2016, pp. 1–23, https://doi.org/10.1016/B978-0-323-42868-2.00001-2.

[26] S. Rondinini, S. Ardizzone, G. Cappelletti, A. Minguzzi, A. Vertova, Materials | sol–gel synthesis. Encyclopedia of Electrochemical Power Sources, Elsevier, 2009, pp. 613–624, https://doi.org/10.1016/B978-044452745-5.00054-X.

[27] M. Hasanzadeh, N. Shadjou, E. Omidinia, M. Eskandani, M. de la Guardia, Mesoporous silica materials for use in electrochemical immunosensing, TrAC Trends Anal. Chem. 45 (2013) 93–106, https://doi.org/10.1016/j.trac.2012.12.017.

[28] Y. Wang, F. Caruso, Mesoporous silica spheres as supports for enzyme immobilization and encapsulation, Chem. Mater. 17 (2005) 953–961, https://doi.org/10.1021/cm0483137.

[29] K. Möller, T. Bein, Degradable drug carriers: vanishing mesoporous silica nanoparticles, Chem. Mater. 31 (2019) 4364–4378, https://doi.org/10.1021/acs.chemmater.9b00221.

[30] A. Bakhshian Nik, H. Zare, S. Razavi, H. Mohammadi, P. Torab Ahmadi, N. Yazdani, M. Bayandori, N. Rabiee, J. Izadi Mobarakeh, Smart drug delivery: Capping strategies for mesoporous silica nanoparticles, Microporous Mesoporous Mater. 299 (2020) 110115, https://doi.org/10.1016/j.micromeso.2020.110115.

[31] E. Molina, M. Mathonnat, J. Richard, P. Lacroix-Desmazes, M. In, P. Dieudonné, T. Cacciaguerra, C. Gérardin, N. Marcotte, pH-mediated control over the mesostructure of ordered mesoporous materials templated by polyion complex micelles, Beilstein J. Nanotechnol. 10 (2019) 144–156, https://doi.org/10.3762/bjnano.10.14.

[32] L. Contessotto, E. Ghedini, F. Pinna, M. Signoretto, G. Cerrato, V. Crocellà, Hybrid organic–inorganic silica gel carriers with controlled drug-delivery properties, Chem. – A Eur. J. 15 (2009) 12043–12049, https://doi.org/10.1002/chem.200900603.

[33] E. Ghedini, V. Nichele, M. Signoretto, G. Cerrato, Structure-directing agents for the synthesis of TiO_2 -based drug-delivery systems, Chem. – A Eur. J. 18 (2012) 10653–10660, https://doi.org/10.1002/chem.201201355.

[34] S.K. Jana, A. Mochizuki, S. Namba, Progress in pore-size control of Mesoporous MCM-41 molecular sieve using surfactant having different alkyl chain lengths and various organic auxiliary chemicals, Catal. Surv. Asia 8 (2004) 1–13, https://doi.org/10.1023/B:CATS.0000015110.85694.d9.

[35] V. Gold, ed., The IUPAC Compendium of Chemical Terminology, International Union of Pure and Applied Chemistry (IUPAC), Research Triangle Park, NC, 2019. https://doi.org/10.1351/goldbook.

[36] S.-H. Wu, C.-Y. Mou, H.-P. Lin, Synthesis of mesoporous silica nanoparticles, Chem. Soc. Rev. 42 (2013) 3862, https://doi.org/10.1039/c3cs35405a.

[37] H.-P. Lin, C.-Y. Mou, Structural and morphological control of cationic surfactant-templated mesoporous silica, Acc. Chem. Res 35 (2002) 927–935, https://doi.org/10.1021/ar000074f.

[38] R. Narayan, U. Nayak, A. Raichur, S. Garg, Mesoporous silica nanoparticles: a comprehensive review on synthesis and recent advances, Pharmaceutics 10 (2018) 118, https://doi.org/10.3390/pharmaceutics10030118.

[39] Z. ALOthman, A review: fundamental aspects of silicate mesoporous materials, Materials 5 (2012) 2874–2902, https://doi.org/10.3390/ma5122874.

[40] S. Kumar, M.M. Malik, R. Purohit, Synthesis methods of mesoporous silica materials, Mater. Today Proc. 4 (2017) 350–357, https://doi.org/10.1016/j.matpr.2017.01.032.

[41] A. Maleki, H. Kettiger, A. Schoubben, J.M. Rosenholm, V. Ambrogi, M. Hamidi, Mesoporous silica materials: from physico-chemical properties to enhanced dissolution of poorly water-soluble drugs, J. Control. Release 262 (2017) 329–347, https://doi.org/10.1016/j.jconrel.2017.07.047.

[42] R.K. ILER, The colloid chemistry of silica and silicates, Soil Sci. 80 (1955) 86, https://doi.org/10.1097/00010694-195507000-00014.

[43] A. Rimola, D. Costa, M. Sodupe, J.-F. Lambert, P. Ugliengo, Silica surface features and their role in the adsorption of biomolecules: computational modeling and experiments, Chem. Rev. 113 (2013) 4216–4313, https://doi.org/10.1021/cr3003054.

[44] C. Pizzolitto, E. Ghedini, F. Menegazzo, M. Signoretto, A. Giordana, G. Cerrato, G. Cruciani, Effect of grafting solvent in the optimisation of Sba-15 acidity for levulinIc acid production, Catal. Today 345 (2020) 183–189, https://doi.org/10.1016/j.cattod.2019.11.012.

[45] M. Balouiri, M. Sadiki, S.K. Ibnsouda, Methods for in vitro evaluating antimicrobial activity: a review, J. Pharm. Anal. 6 (2016) 71–79, https://doi.org/10.1016/j.jpha.2015.11.005.

[46] F.A. Arzani, J.H.Z. dos Santos, Biocides and techniques for their encapsulation: a review, Soft Matter 18 (2022) 5340–5358, https://doi.org/10.1039/D1SM01114F.

[47] A. Michaelsen, F. Pinzari, N. Barbabietola, G. Piñar, Monitoring the effects of different conservation treatments on paper-infecting fungi, Int Biodeterior. Biodegrad. 84 (2013) 333–341, https://doi.org/10.1016/j.ibiod.2012.08.005.

[48] A. Ramirez, J.-M. Clacens, C. Lorentz, Y. Pouilloux, Comparison between SBA-15 and MCM-41 structure on the stability and the selectivity of basic catalysts in oligomerization of glycerol, Curr. Org. Chem. 16 (2012) 2774–2781, https://doi.org/10.2174/138527212804546903.

[49] M. Thommes, R. Köhn, M. Fröba, Sorption and pore condensation behavior of pure fluids in mesoporous MCM-48 silica, MCM-41 silica, SBA-15 silica and controlled-pore glass at temperatures above and below the bulk triple point, Appl. Surf. Sci. 196 (2002) 239–249, https://doi.org/10.1016/S0169-4332(02)00062-4.

[50] I. Díaz, F. Mohino, J. Pérez-Pariente, E. Sastre, Study by TG–MS of the oxidation of SH-MCM-41 to SO3H-MCM-41, Thermochim. Acta 413 (2004) 201–207, https://doi.org/10.1016/j.tca.2003.10.008.